CHEMISTRY
AN ASIAN JOURNAL
www.chemasianj.org

Accepted Article

Title: A Hollow Microtubular Triazine- and Benzobisoxazole-Based Covalent Organic Framework Presenting Sponge-Like Shells That Functions as a High-Performance Supercapacitor

Authors: Shiao-Wei Kuo, Ahmed F. M. EL-Mahdy, Ying-Hui Hung, Tharwat Hassan Mansoure, Hsiao-Hua Yu, and Tao Chen

To be cited as: *Chem. Asian J.* 10.1002/asia.201900296

Link to VoR: http://dx.doi.org/10.1002/asia.201900296

A Journal of
ACES Asian Chemical Editorial Society

A sister journal of Angewandte Chemie and Chemistry – A European Journal

WILEY-VCH

10.1002/asia.201900296
WILEY-VCH

A Hollow Microtubular Triazine- and Benzobisoxazole-Based Covalent Organic Framework Presenting Sponge-Like Shells That Functions as a High-Performance Supercapacitor

Ahmed F. M. EL-Mahdy, Ying-Hui Hung, Tharwat Hassan Mansoure, Hsiao-Hua Yu, Tao Chen, Shiao-Wei Kuo*

Abstract: In this paper we report the construction of a hollow microtubular triazine- and benzobisoxazole-based covalent organic framework (COF) presenting a sponge-like shell through the template-free [3+2] condensation of the planar molecules 2,4,6-tris(4-formylphenyl)triazine (TPT-3CHO) and 2,5-diaminohydroquinone dihydrochloride (DAHQ-2HCl). The synthesized COF exhibited extremely high crystallinity, a high surface area (ca. 1855 m^2 g^{-1}), and ultrahigh thermal stability. Interestingly, a time-dependent study of the formation of the hollow microtubular COF having a sponge-like shell revealed a transformation from initial ribbon-like crystallites into the hollow tubular structure, and confirmed that the hollow nature of the synthesized COF was controlled by inside-out Ostwald ripening, while the non-interaction of the crystallites on the outer surface was responsible for the sponge-like surface of the tubules. This COF exhibited significant supercapacitor performance: a high specific capacitance of 256 F g^{-1} at a current density of 0.5 A g^{-1}, excellent cycling stability (98.8% capacitance retention over 1850 cycles), and a high energy density of 43 W h kg^{-1}. Such hollow structural COFs with sponge-like shells appear to have great potential for use as high-performance supercapacitors in energy storage applications.

Supercapacitors[1] are energy storage devices, also known as electric double-layer capacitors, that have wide appeal for their massive power densities, operation over a broad range of temperatures, extra-long life times, and high reversibility. According to the nature of the electrode material and the mechanism of energy storage, supercapacitors can store energy through either faradaic or non-faradaic processes.[2,3] In the faradaic process, energy storage occurs via electron transfer across the electrolyte–electrode interface, due to the rapid and reversible reduction/oxidation (redox) processes of the specific materials supported on the electrode surface; such materials are also known as pseudocapacitors.[4] In the non-faradaic process, however, the energy storage occurs via frequent adsorption/desorption of charged electrolyte ions on the tiny surface of the electrode; no charge transfer occurs.[2-4] In both of these processes, the electrode material has the main effect on the efficiency of the capacitor. For the non-faradaic process, high-performance electrode materials possessing geometrical porous structures and high surface areas are necessary to enhance the transfer of the charged electrolyte ions. In many previous carbons, activated carbons, graphene aerogels, and porous graphene[5]—have been used to dramatically enhance the effectiveness of supercapacitors. Furthermore, doping nitrogen heteroatoms into these carbon materials can also greatly improve the efficiency of supercapacitors, through the pseudocapacitance effect supplied by the nitrogen atom;[6] in addition, the nitrogen atoms affect the electron distribution of the carbon atoms and, thereby, enhance both the electroactivity and wettability of the surface area—a so-called heteroatom effect.[7] Recently, conjugated microporous polymer materials (CMPs) have been developed with the intent to enhance the efficiency of the supercapacitors.[8] In addition, porous frameworks materials—namely, covalent organic frameworks (COFs) and metal-organic frameworks (MOFs), which have uniform nanoscale pore sizes, specific crystalline networks, and various modes of heteroatom doping—have displayed excellent performance when used within supercapacitors.[9] Nevertheless, the application of COFs within electrochemical devices has many challenges arising from their weak oxidative and hydrolytic stabilities, especially in the case of COFs containing boronic ester linkages.[9a,b]

COFs are porous crystalline frameworks that are constructed through the assembly of organic building blocks (linkers)

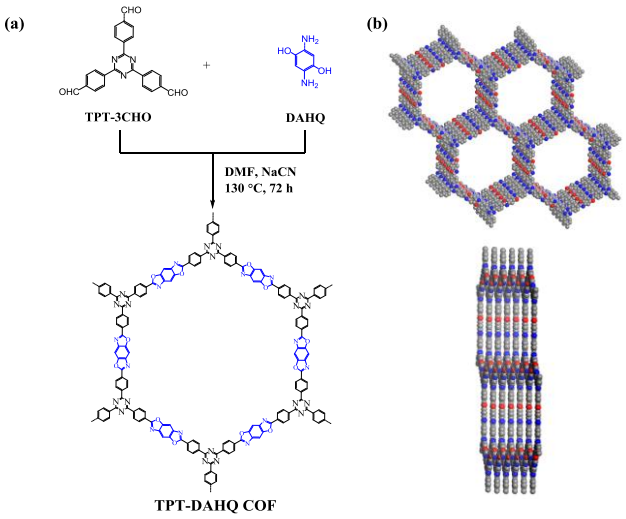

Figure 1. (a) Schematic presentation of the preparation of TPT-DAHQ COF and (b) Top and side sights of the AA-stacking model of TPT-DAHQ COF.

Dr. A. F. M. EL-Mahdy, Y.-H. Hung, Prof. Dr. S.-W. Kuo*
Department of Materials and Optoelectronic Science, Center of Crystal Research, National Sun Yat-Sen University, Kaohsiung 80424, Taiwan
E-mail: kuosw@faculty.nsysu.edu.tw
Dr. A. F. M. EL-Mahdy, T. H. Mansoure
Chemistry Department, Faculty of Science, Assiut University, Assiut 71516, Egypt.
Dr. H.-H. Yu, T. H. Mansoure
Institute of Chemistry, Academia Sinica, 128 Academic Road, Sec. 2, Nankang, Taipei 11529, Taiwan
Nanoscience and Technology Program, Taiwan International Graduate Program, Academia Sinica and National Taiwan University, Taipei 11529, Taiwan
Department of Chemistry, National Taiwan University, Taipei 106, Taiwan
Center for Emergent Functional Matter Science, National Chiao Tung University, Hsinchu 30010, Taiwan
Prof. Dr. T. Chen
Ningbo Institute of Material Technology and Engineering, Chinese Academy of Science, Zhongguan West Road 1219, 315201 Ningbo, China
Prof. Dr. S.-W. Kuo
Department of Medicinal and Applied Chemistry, Kaohsiung Medical University, Kaohsiung 807, Taiwan

10.1002/asia.201900296
WILEY-VCH

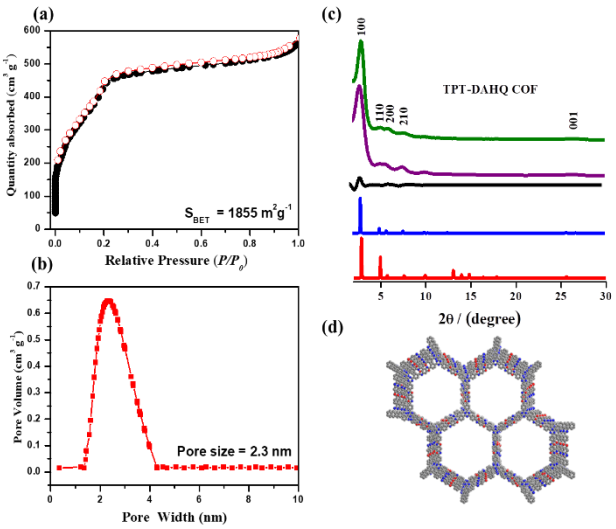

Figure 2. (a) N_2 gas adsorption (●) and desorption (○) isotherms and (b) pore size distribution curve of the TPT-DAHQ COF. (c) PXRD pattern of the TPT-DAHQ COF: experimental (green), Pawley refined (purple), difference between the experimental and calculated data (black), calculated for the AA-stacking model (blue) and AB-stacking model (red). (d) Three-dimensional space-filling structure for the AA-stacking model.

connected through stable covalent bonds. Because of their excellent crystallinity, permanent porosity, high surface areas, and thermal stability,[9a,b–10] COFs have potential applications in such fields as catalysis, gas storage and separation, optoelectronics, and energy storage.[11] Although COFs have been constructed from a wide selection of linkers, most have been obtained as crystalline powders with various shapes, including sheets, cubes, belts, fibers, prisms, and platelets.[12] The self-assembly of porous crystallites into spherical or tubular structures within polymeric materials has received great attention for their applications in sensors, catalysis, energy storage, and drug delivery.[13] The synthesis and isolation of COFs having hollow spherical or tubular shapes has been rare. The reported COFs possessing spherical or tubular shapes have been synthesized using templated and template-free strategic methods. In the reported templated methods, the COF was first grown on the surface of a metal oxide possessing a spherical or tubular shape, and then the metal oxide was removed.[14] In the template-free approaches, the COFs were first formed as small crystallites that self-assembled into spherical or tubular shapes, in the absence of a template; the construction of COFs through this method has, however, been exceedingly rare.[15]

In this study, we synthesized crystalline covalent benzobisoxazole- and triazine-based organic framework and applied it within electrochemical supercapacitors. Benzobisoxazoles are the monomer units of polybenzoxazoles, which are heterocyclic and rod-like polymers displaying excellent thermal stability, low dielectric constants, great chemical resistance, and lower water absorption because they have no polar groups in the polymer backbones.[16] Therefore, polybenzoxazoles are being used widely in the semiconductor industry: in integrated chips, in high-end electronic packaging materials, and in a variety of photoelectric devices.[17] Triazine building blocks are used to prepare covalent triazine frameworks (CTFs), which are microporous organic frameworks containing nitrogen heteroatoms that are formed through the trimerization of nitrile groups under ionothermal conditions. Although CTFs have functioned as excellent electrodes in capacitors and lithium-sulfur batteries,[18] due to their high surface areas and well-arranged and size-distributed pores, they have not possessed crystalline structures. In this paper we report a benzobisoxazole- and triazine-based COF having a hollow tubular structure and presenting a sponge-like shell, synthesized through a [3+2] condensation of the planar molecules 2,4,6-tris(4-formylphenyl)triazine (TPT-3CHO) and 2,5-diaminohydroquinone dihydrochloride (DAHQ-2HCl) (Figure 1). We also describe the mechanism of formation of the hollow tubules presenting the sponge-like shells, and the supercapacitor efficiency of this COF.

Our benzobisoxazole- and triazine-based COF possessing high porosity, high crystallinity, and ultrahigh thermal stability was prepared through a sequence of Schiff base formation, nucleophilic addition, and aerobic oxidation. The TPT-DAHQ COF was synthesized in a Pyrex tube through one-pot solvothermal condensation between TPT-3CHO (Figures S1–S4) and DAHQ-2HCl in *N*,*N*-dimethylformamide (DMF), over 72 h at 120 °C. As reported previously, the formation of the benzoxazole ring presumably occurred in a three-step sequence (Scheme S1): (i) formation of a phenolic Schiff base intermediate, (ii) nucleophilic addition of the cyanide nucleophile to the imino (C=N) bond to accelerate ring cyclization and the formation of a benzoxazoline intermediate, and (iii) formation of the benzoxazole ring upon aerobic oxidation of the benzoxazoline intermediate.[19]

The formation of benzoxazole rings and the synthesis of TPT-DAHQ COF were confirmed using Fourier transform infrared (FTIR) spectroscopy, solid state ^{13}C cross-polarization (CP)/magic angle spinning (MAS) NMR spectrum, and elemental analysis. The FTIR spectrum of DAHQ-2HCl (Figure S5) was characterized by a broad signal near 3200 cm^{-1}, attributed to the phenolic (OH) and ammonium (NH_3Cl) units, in addition to other peaks at 1555 cm^{-1} for the aromatic (C=C) groups, 1352 cm^{-1} for C–N bending, and 1190 cm^{-1} for C–O bending. The FTIR spectrum of TPT-3CHO was characterized by signals for the aldehydic (C=O) groups at 1706 cm^{-1}, triazine (C=N) groups at 1608 cm^{-1}, and aromatic (C=C) groups at 1583 and 1517 cm^{-1}. The FTIR spectrum of the synthesized TPT-DAHQ COF lacked any of the signals for the phenolic (OH), ammonium (NH_3Cl), and aldehydic (C=O) groups of the DAHQ-HCl and TPT-3CHO monomers, but did feature peaks at 1613 and 1117 cm^{-1} representing the stretching of the C=N and C–O units of benzoxazole rings,[20] confirming the formation of the benzobisoxazole- and triazine-based COF. The composition and atomic structure of the TPT-DAHQ COF was confirmed through solid state ^{13}C CP/MAS NMR spectroscopy and elemental analysis. As revealed in Figure S4, the ^{13}C NMR spectrum of the TPT-3CHO monomer was characterized by two specific peaks: at 191.48 ppm, for the aldehydic (C=O) groups, and at 170.47 ppm, for the triazine unit. The solid state ^{13}C NMR spectrum of TPT-DAHQ COF lacked the signal for the aldehydic (C=O) groups, but featured three peaks at 162.36, 148.18, and 140.36 ppm corresponding to the resonances of the benzoxazole ring.[20] The peak at 169.26 ppm arose from the triazine unit (Figure S6). Elemental analysis data from the TPT-DAHQ COF was concordant with the theoretical value for its two-dimensional (2D) sheets (Table S1). Furthermore, thermogravimetric analysis (TGA) of TPT-DAHQ COF revealed that it was extraordinarily thermally stable up to 452 °C under a N_2 atmosphere (Figure S7, Table S2). The synthesized TPT-DAHQ COF maintained approximately 95 and 90% of its weight after heating to 380 and 452 °C, respectively, under a N_2 atmosphere. Together, the

10.1002/asia.201900296

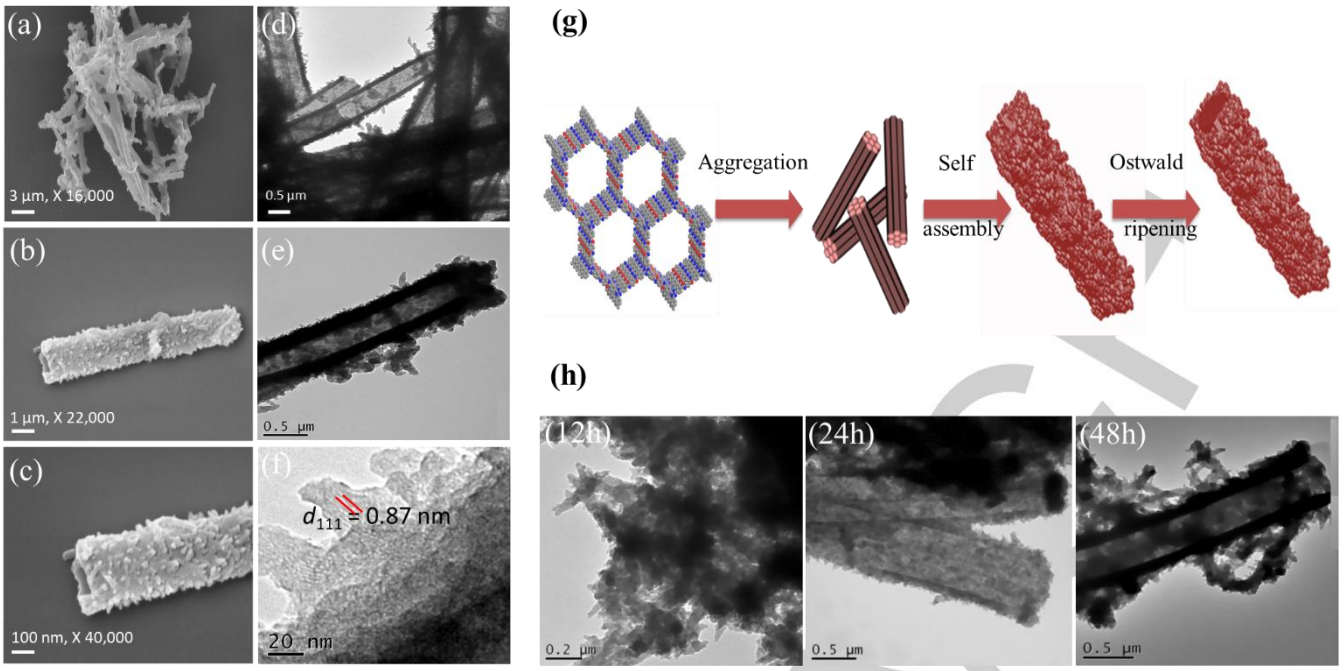

Figure 3. (a–c) FE-SEM and (d–f) TEM images of the hollow microtubular TPT-DAHQ COF having sponge-like shells, recorded at various magnifications. (g) Expected mechanism of formation of the hollow microtubular TPT-DAHQ COF having sponge-like shells. (h) TEM images of the hollow microtubular TPT-DAHQ COF having sponge-like shells, measured after reaction times of 12, 24, and 48 h.

results above confirmed the formation of the benzobisoxazole- and triazine-based COF.

We performed N_2 adsorption and desorption measurements of our synthesized TPT-DAHQ COF at 77 K to study its permanent porosity. As presented in Figure 2a, the sorption isotherm of TPT-DAHQ COF exhibited a type IV isothermal behavior that is characteristic of mesoporous polymers. We used the Brunauer–Emmett–Teller (BET) model to calculate the surface area of the TPT-DAHQ COF; we obtained a BET surface area of 1855 $m^2\ g^{-1}$ and a pore volume of 0.7 $cm^3\ g^{-1}$. Using nonlocal density functional theory, we estimated the pore size distribution of the TPT-DAHQ COF, obtaining an approximate pore size of 2.3 nm (Figure 2b). The previously reported benzobisoxazole-linked COFs BBO-COF 1 and 2, and LZU-191 had BET surface areas of 891, 1106, and 1305 $m^2\ g^{-1}$, respectively, and pore sizes of 1.34, 1.84, and 2.3 nm, respectively.[20] Thus, our synthesized benzobisoxazole- and triazine-based COF had a relatively larger BET surface area. We used powder X-ray diffraction (PXRD) and computational simulations to gain insight into the crystalline structure of the TPT-DAHQ COF. The experimental PXRD pattern of the TPT-DAHQ COF featured a massive XRD peak at a value of 2θ of 2.90°, and four others at 5.05, 5.86, 7.69, and 26.04°, corresponding to the (100), (110), (200), (210), and (001) reflections, respectively (Figures 2c and S8). In addition, according to the Bragg equation, the *d*-spacing between the 100 planes (d_{100}) of the TPT-DAHQ COF and the π-stacking interlayer distance between its 2D sheets 2.9 nm and 3.4 Å, respectively. Simulation, using the software Material Studio (v. 7.0), of the crystalline structure and the PXRD pattern of the TPT-DAHQ COF provided a simulated PXRD pattern yielded from the Pawley refinement (Figure 2c, purple curve) that was very similar to the experimental PXRD pattern (Figure 2c, green curve), as evidenced by their difference pattern (Figure 2c, black curve). In addition, the AA-eclipsed stacking model of the TPT-DAHQ COF produced an XRD pattern (Figure 2c, blue curve) that matched well with the experimental pattern, while the AB-eclipsed stacking model produced an XRD pattern (Figure 2c, red curve) that deviated largely from the experimental pattern. The refined unit cell of the TPT-DAHQ COF provided the following cell parameters: $a = b = 35.6565$ Å; $c = 3.4790$ Å; $\alpha = \beta = 90°$; $\gamma = 120°$ (residuals $R_{wp} = 10.14\%$; $R_p = 8.26\%$) (Figures S9 and S10, Table S3). These findings confirmed the formation of a 2D crystalline framework having a regular hexagonal and honeycomb-type lattice.

We applied field-emission scanning electron microscopy (FE-SEM) and transmission electron microscopy (TEM) to investigate the morphology of the TPT-DAHQ COF. The FE-SEM images of the TPT-DAHQ COF revealed the formation of hollow tubular structures having an average length of 7.4 µm and an average diameter of 1 µm (Figures 3a–c). Interestingly, the outer shell of the tubular TPT-DAHQ COF contained a very large number of nanowires, which were branched and spread in various directions, forming an interconnected microsponge structure. The TEM images of the synthesized COF confirmed its hollow nature and sponge-like surface of tubules. In Figures 3d–e, the tubule's center appears as a bright area and its outer surface as a dark area—a basic characteristic feature of a hollow structure;[15c] the nanowires on the outer surface were responsible for the formation of the sponge-like structure.[21] Statistical analysis of the TEM images provided average values for the outer and inner diameters of the tubules of 0.90 and 0.53 µm, respectively. The lower-magnification TEM image revealed the rhomboidal framework of the TPT-DAHQ COF and lattice borders having a *d*-spacing of 0.87 nm, corresponding to the (111) plane of the framework (Figure 3f). Comparing to the chemical similarity structure LZU-191 COF which was prepared through the reaction of TPT-3CHO and DAHQ-2HCl in co-solvent of *N*-methyl-2-pyrrolidone (NMP) and mesitylene for 5 days (120 h) in the presence of benzimidazole as catalyst,[20b] our TPT-DAHQ COF was prepared in homosolvent of DMF for 72 h in the presence of NaCN as a catalyst. Interestingly, our new method improved the BET surface area of resultant COF to be

10.1002/asia.201900296

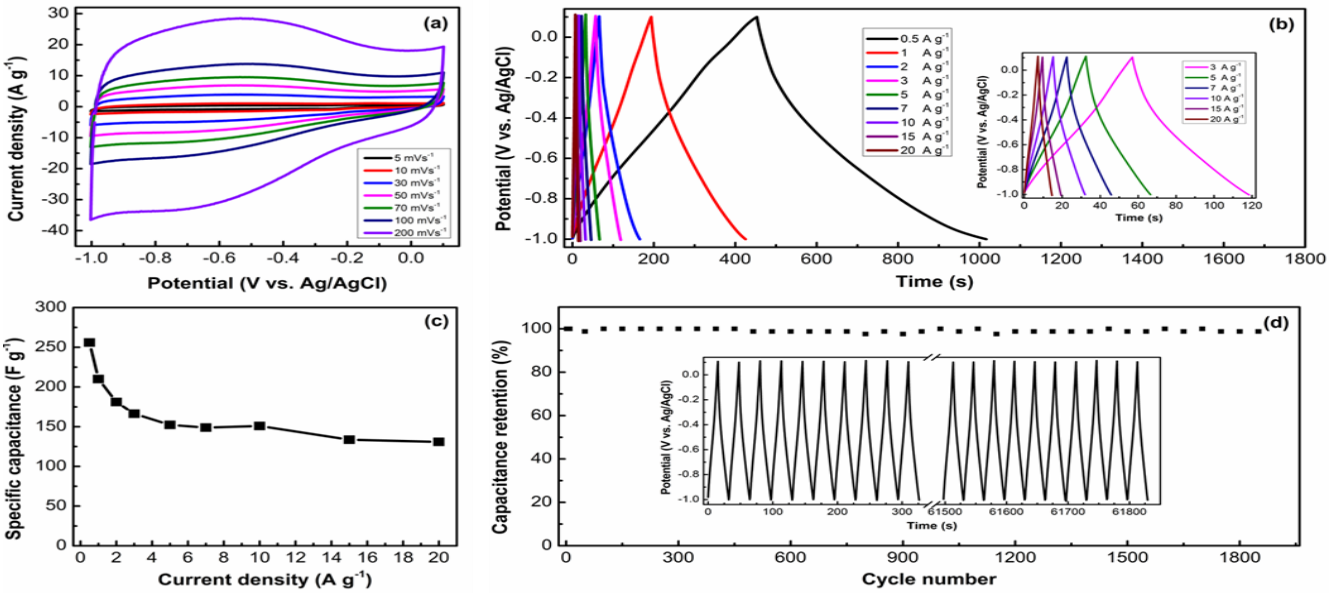

Figure 4. Electrochemical performance of the TPT-DAHQ COF electrode in 1 M KOH, measured using a three-electrode system: (a) CV curves recorded at various scan rates, (b) galvanostatic charge–discharge curves recorded at various current densities, (c) corresponding specific capacitances recorded at various current densities, and (d) cycling performance recorded at a current density of 10 A g^{-1}, with the first and last 10 cycles of the galvanostatic charge–discharge curves inserted.

1855 m^2 g^{-1} and lead to the formation of the hollow microtubular COF having a sponge-like shell.

To investigate the mechanism of formation of the hollow microtubules, we examined their morphologies at various reaction times (12, 24, and 48 h) during the synthesis of the TPT-DAHQ COF. Here, we synthesized the TPT-DAHQ COF under the same conditions we had used previously, but quenched the reaction at those specific times by removing the Pyrex tube from the oil bath and cooling it to room temperature. The resultant COFs were isolated, washed with THF and acetone, and they subjected to TEM imaging (Figure 3h). The TEM image of the sample after 12 h revealed an aggregation of tiny planar ribbon-like crystallites having widths in the range 40–50 nm. These planar crystallites could have arisen from high degrees of π-stacking between layers of the TPT-DAHQ COF (Figure 3h). Interestingly, after a reaction time of 24 h, these planar crystallites had self-assembled with a strong penchant to form dark and dense tubular structures. Nevertheless, the higher-magnification image (Figure 3h) revealed individual ribbon-like crystallites, which acted as building units of the tubules, on the outer shells of the tubules. The TEM image of the TPT-DAHQ COF after a reaction time of 48 h revealed the migration of the ribbon-like crystallites from the tubular centers to their outer shells, resulting in the formation of hollow gaps within the dense tubules (Figure 3h). As previously reported, this kind of hollow structure is usually induced through an inside-out Ostwald ripening process, in which the crystallites migrate from the inner center, where the crystallites have higher surface energy, to the outer shell, to decrease their surface energy.[13b,22] The formation of a COF having a hollow tubular structure through a mechanism of inside-out Ostwald ripening is, however, exceptional and rare.[12,15a,b] Furthermore, the outer shells of these hollow tubules were not smooth, with the ribbon-like crystallite building blocks still present. After a complete reaction time of 72 h, the morphology remained that of hollow microtubules having a sponge-like surface (Figure 3d-f). The sponge-like outer shell might have arisen from the presence of only one kind of terminal functional group (e.g., amino groups) on the surfaces of the ribbon-like crystallites, thereby not allowing further reactions among the crystallites. As reported previously, the formation of a smooth surface requires reactions between the crystallites themselves, those present on the surface, through two different terminal functional groups (e.g., aldehydic and amino groups).[15a] Thus, TEM imaging of the TPT-DAHQ COF formed after various reaction times suggested that its hollow structures were controlled through inside-out Ostwald ripening and that the sponge-like surfaces of the tubules resulted from a lack of covalent interaction among the crystallites on the outer surface (Figure 3g). Additionally, we examined the PXRD patterns of the resultant COF at different reaction times (12, 24, and 48 h) during the synthesis of the TPT-DAHQ COF. As presented in Figure S11, TPT-DAHQ COF crystallites are completely formed even at short reaction time, indicating the following and accompanying self-assembly and inside-out Ostwald ripening of these COF crystallites did not destroyed the internal ordering of the COF.

We investigated the electrochemical performance of the TPT-DAHQ COF through cyclic voltammetry (CV) using a three-electrode system in 1 M aqueous KOH. Figure 4a presents the CV curves of the TPT-DAHQ COF recorded at various scan rates, from 5 to 200 mV s^{-1}. The CV curves all had rectangular shapes, even when recorded at the highest scan rate of 200 mV s^{-1}, suggesting capacitive behavior with a high rate performance suitable for use in supercapacitors.[5b,8,23] The distinct appearance of humps in the rectangular CV curves revealed that the capacitive response was derived from a combination of electric double-layer capacitance (EDLC) and pseudocapacitance arising from the presence of heteroatoms (i.e., nitrogen and oxygen atoms).[7a,24a] Figure 4b provides galvanostatic charge–discharge (GCD) curves of the TPT-DAHQ COF recorded at various current densities, from 0.5 to 20 A g^{-1}. The GCD curves display triangular shapes with a slight bend, implying the existence of both EDLC and pseudocapacitance arising from heteroatoms (i.e., nitrogen and oxygen atoms).[5b,23,24a] The specific capacitance was calculated from the GCD curves using equation (S1) as shown in Figure 4c. The

10.1002/asia.201900296

TPT-DAHQ COF exhibited excellent specific capacitance of 256 F g^{-1} at current density of 0.5 A g^{-1} which was decreased to 131 F g^{-1} when the current density was increased to 20 A g^{-1}. This excellent performance could be attributed to the higher surface area (1855 m^2 g^{-1}) and the existence of mesoporosity (pore size of 2.3 nm) along with the presence of heteroatoms (nitrogen and oxygen), which enable easier accessibility of electrolytes to the electrode surface.[24a,b] The reported specific surface area and specific capacitance values are summarized in Table S4. The durability of the TPT-DAHQ COF electrode was tested by cycling at 10 A g^{-1} for 1850 cycles as shown in Figure 4d. Remarkably, TPT-DAHQ COF showed excellent cycling stability without obvious degradation of capacitance after 1850 cycles. As shown in Figure 4d, the specific capacitance of the TPT-DAHQ COF retains 98.8% of its original capacitance after 1850 cycles. Recently, Liao *et al*. reported COF-0d, COF-5d, and Fe_3O_4/COF-5d having capacitances of 64, 52, and 112 F g^{-1} at 0.5 A g^{-1}, respectively, which showed capacitance retention of 52, 77, and 76%, respectively, after 2000 cycles at 5 A g^{-1}.[20a] In addition, DeBlase *et al.* reported DAAQ-TFP COF with a capacitance of 48 ± 10 F g^{-1} at 0.1 A g^{-1}, which stabilized at 40 ± 9 Fg^{-1} after 10 GCD cycles, after which no further significant decrease was observed after 5000 cycles.[11d] Bhanja *et al.* reported TDFP-1 exhibiting a capacitance of 418 F g^{-1} at 0.5 A g^{-1} with 95% capacitance retention after 1000 cycles at 10 A g^{-1}.[25a] Moreover, Das *et al.* reported TFP-NDA-COF with a capacitance of 348 F g^{-1} at 0.5 A g^{-1}, which retained 75% of its initial capacitance after 8000 cycles.[25b] These results confirmed that our DAAQ-TFP COF is among the highest previously reported COFs (Table S4). In addition, these results confirmed our recently conception[15a] which mentioned that the structure morphology of a COF material plays an important role to enhance the specific capacitance. Within TPT-DAHQ COF, tubular structure provides large surface area and numerous pore sizes, which enables fast ions diffusion and electrode-electrolyte contact during the electrochemical process. Thus, the molecular design of COFs (i.e. redox groups, porosity, morphology, conjugated structure, etc.) is important and control the supercapacitor application. Furthermore, our TPT-DAHQ COF exhibited excellent capacitance among the most reported mesoporous materials such as conjugated microporous polymers (CMP) with capacitances of 141 F g^{-1} and 183 F g^{-1} at 1 A g^{-1},[8a] metal-organic frameworks (MOFs) with capacitances of 1200, 300, and 400 F g^{-1} at 1 A g^{-1},[9f] nitrogen-doped porous carbon-nanosheets with capcitance of 128 F g^{-1} at 0.1 A g^{-1},[26a] nitrogen-doped carbon nanoparticles with capacitance of 84 F g^{-1} at 1 A g^{-1},[26b] sulfur /nitrogen co-doped mesoporous carbon with capacitance of 160 F g^{-1} at 1 A g^{-1}[26c] and copolymer-templated nitrogen-porous carbons with capacitance of 166 F g^{-1} at 0.1 A g^{-1}.[26d]

In conclusion, we have report the successfully synthesis of a hollow microtubular triazine- and benzobisoxazole-based covalent organic framework—TPT-DAHQ COF with a sponge-like shell—through a template-free [3+2] condensation of the planar molecules TPT-3CHO and DAHQ-2HCl. The resultant TPT-DAHQ COF exhibited high BET surface areas (up to ca. 1855 m^2 g^{-1}), excellent crystallinity, and high thermal stability (up to ca. 450 °C). FE-SEM and TEM imaging were utilized to investigated the mechanism of formation of the hollow microtubular COF having a sponge-like shell by studying the morphological changes in TPT-DAHQ COF at different times during its preparation. This time-dependent study exhibited that the hollow nature of the synthesized COF was controlled by inside-out Ostwald ripening, while the sponge-like surface of the tubules was formed as a result of the non-interaction of the crystallites on the outer surface. In the electrochemical application, TPT-DAHQ COF exhibited a significant supercapacitor performance—with high specific capacitance of 256 F g^{-1} at current density of 0.5 A g^{-1}, excellent cycling stability (98.8% capacitance retention for 1850 cycles), and high energy density of 43 Wh kg^{-1}. We totally believed that such hollow structural COFs with sponge-like shells will open a great domain for using such COFs as high-performance supercapacitors in energy storage applications.

Keywords: triazine • benzobisoxazole • covalent organic framework • sponge • supercapacitor

[1] a) P. Simon, Y. Gogotsi, *Nat. Mater.* **2008**, 7, 845−854; b) H. Nishihara, T. Kyotani, *Adv. Mater.* **2012**, 24, 4473−4498; c) F. Béguin, V. Presser, A. Balducci, E. Frackowiak, *Adv. Mater.* **2014**, 26, 2219−2251; d) G. Zhou, F. Li, H.-M. Cheng, *Energy Environ. Sci.* **2014**, 7, 1307−1338.

[2] a) G. Wang, L. Zhang, J. Zhang, *Chem. Soc. Rev.* **2012**, 41,797−828; b) Y. Peng, Z. Chen, J. Wen, Q. Xiao, D. Weng, S. He, H. Geng, Y. Lu, *Nano Res.* **2011**, 4, 216−225.

[3] A. M. Khattak, H. Yin, Z. A. Ghazi, B. Liang, A. Iqbal, N. A. Khan, Y. Gao, L. Li, Z. Tang, *RSC Adv.* **2016**, 6, 58994−59000.

[4] I. E. Rauda, V. Augustyn, B. Dunn, H. S. Tolbert, *Acc. Chem. Res.* **2013**, 46, 1113−1124.

[5] a) Z. Li, Z. W. Xu, X. H. Tan, H. L. Wang, C. M. B. Holt, T. Stephenson, B. C. Olsen, D. Mitlin, *Energy Environ. Sci.* **2013**, 6, 871−878; b) A. Alabadi, X. Yang, Z. Dong, Z. Li, B. Tan, *J. Mater. Chem. A* **2014**, 2, 11697−11705; c) Z.-S. Wu, Y. Sun, Y.-Z. Tan, S. Yang, X. Feng, K. Müllen, *J. Am. Chem. Soc.* **2012**, 134, 19532−19535; d) Z.-Y. Sui, C. Wang, K. Shu, Q.-S. Yang, Y. Ge, G. G. Wallace, B.-H. Han, *J. Mater. Chem. A* **2015**, 3, 10403−10412; e) H.-M. Cheng, F. Li, *Science* **2017**, 356, 582−583.

[6] D. Hulicova-Jurcakova, M. Kodama, S. Shiraishi, H. Hatori, Z. H. Zhu, G.Q. Lu, *Adv. Funct. Mater.* **2009**, 19, 1800−1809.

[7] a) J. Han, L. L. Zhang, S. Lee, J. Oh, K.-S. Lee, J. R. Potts, J. Ji, X. Zhao, R. S. Ruoff, S. Park, *ACS Nano* **2013**, 7, 19−26; b) D. Hulicova-Jurcakova, A. M. Puziy, O. I. Poddubnaya, F. Suárez-García, J. M. D. Tascón, G. Q. Lu, *J. Am. Chem. Soc.* **2009**, 131, 5026−5027.

[8] a) Y. Kou, Y. Xu, Z. Guo, D. Jiang, *Angew. Chem. Int. Ed.* **2011**, 50, 8753−8757; *Angew. Chem.* **2011**, 123, 8912−8916; b) X.-C. Li, Y. Zhang, C.-Y. Wang, Y. Wan, W.-Y. Lai, H. Pang, W. Huang, *Chem. Sci.* **2017**, 8, 2959−2965.

[9] a) A. P. Côté, A. I. Benin, N. W. Ockwig, M. O'Keeffe, A. J. Matzger, O. M. Yaghi, *Science* **2005**, 310, 1166−1170; b) J. W. Colson, W. R. Dichtel, *Nat. Chem.* **2013**, 5, 453−465; c) X. Feng, X. Ding, D. Jiang, *Chem. Soc. Rev.* **2012**, 41, 6010−6022; d) S. Wan, J. Guo, J. Kim, H. Ihee, D. Jiang, *Angew. Chem., Int. Ed.* **2009**, 48, 5439−5442; e) X. Ding, L. Chen, Y. Honsho, X. Feng, O. Saengsawang, J. Guo, A. Saeki, S. Seki, S. Irle, S. Nagase, V. Parasuk, D. Jiang, *J. Am. Chem. Soc.* **2011**, 133, 14510− 14513; f) Y-Z. Zhang, T. Cheng, Y. Wang, W-Y. Lai, H. Pang, W. Huang, *Adv. Mater.* **2016**, 28, 5242-5248.

[10] a) S.-Y. Ding, W. Wang, Chem. Soc. Rev., 2013, 42, 548−568; b) H.-L. Qian, C.-X. Yang, X.-P. Yan, *Nat. Commun.* **2016**, 7, 12104−12110.

[11] a) S.-Y. Ding, J. Gao, Q. Wang, Y. Zhang, W.−G. Song, C.−Y. Su, W. Wang, *J. Am. Chem. Soc.* **2011**, 133, 19816−19822; b) H. Furukawa, O. M. Yaghi, *J. Am. Chem. Soc.* **2009**, 131, 8875−8883; c) A. F. M. EL-Mahdy, C.-H. Kuo, A. Alshehri, C. Young, Y. Yamauchi, J. Kim, S.-W. Kuo, *J. Mater. Chem. A* **2018**, 6, 19532−19541; d) C. R. DeBlase, K. E. Silberstein, T.−T. Truong, H. D. Abruña, W. R. Dichtel, *J. Am. Chem. Soc.* **2013**, 135, 16821−16824; e) C. Wu, Y. Liu, H. Liu, C. Duan, Q. Pan, J. Zhu, F. Hu, X. Ma, T. Jiu, Z. Li, Y. Zhao, *J. Am. Chem. Soc.* **2018**, 140, 10016−10024.

[12] a) S. Chandra, S. Kandambeth, B. P. Biswal, B. Lukose, S. M. Kunjir, M. Chaudhary, R. Babarao, T. Heine, R. Banerjee, *J. Am. Chem. Soc.* **2013**, 135, 17853−17861; b) S. Wan, J. Guo, J. Kim, H. Ihee, D. Jiang, Angew. Chem. Int. Ed. 2009, 48, 5439; c) W. Huang, Y. Jiang, X. Li, X.

10.1002/asia.201900296

Li, J. Wang, Q. Wu, X. Liu, *ACS Appl. Mater. Interfaces* **2013**, 5, 8845−8849; d) E. L. Spitler, W. R. Dichtel, *Nat. Chem.* **2010**, 2, 672−677; e) H. M. El-Kaderi, J. R. Hunt, J. L. Mendoza-Cortés, A. P. Côté, R. E. Taylor, M. O'Keeffe, O. M. Yaghi, *Science* **2007**, 316, 268−272.

[13] a) L. Zhou, Z. Zhuang, H. Zhao, M. Lin, D. Zhao, L. Mai, *Adv. Mater.* **2017**, 29, 1602914; b) X. W. Lou, L. A. Archer, Z. Yang, *Adv. Mater.* **2008**, 20, 3987−4019; c) L. Hu, Q. Chen, *Nanoscale* **2014**, 6, 1236−1257; d) K. Jiang, X. Zhang, J. Huang, S. Wang, J. Chen, *J. Electroanal. Chem.* **2017**, 796, 88−95.

[14] P. Pachfule, S. Kandmabeth, A. Mallick, R. Banerjee, *Chem. Commun.* **2015**, 51, 11717−11720.

[15] a) A. F. M. EL-Mahdy, C. Young, J. Kim, J. You, Y. Yamauchi, S. W. Kuo, ACS Appl. Mater. Interfaces 2019, DOI: 10.1021/acsami.8b21867; b) S. Kandambeth, V. Venkatesh, D. B. Shinde, S. Kumari, A. Halder, S. Verma, R. Banerjee, Nat. Commun. 2015, 6, 6786; c) A. Halder, S. Kandambeth, B. P. Biswal, G. Kaur, N. C. Roy, M. Addicoat, J. K. Salunke, S. Banerjee, K. Vanka, T. Heine, S. Verma, R. Banerjee, Angew. Chem. Int. Ed. 2016, 55, 7806; d) B. Gole, V. Stepanenko, S. Rager, M. Grgne, D. D. Medina, T. Bein, F. Wgrthner, and F. Beuerle, Angew. Chem. Int. Ed. 2018, 57, 846.

[16] a) M. Ueda, T. Nakayama, *Macromolecules* **1996**, 29, 6427−6431; b) H. Makabe, T. Banba, T. Hirano, *J. Photopolym. Sci. Technol.* **1997**, 10, 307−312.

[17] T. D. Dang, P. T. Mather, M. D. Alexander, C. J. Grayson, M. D. Houtz, R. J. Spry, F. E. Arnold, *J. Polym. Sci. Polym. Chem.* **2000**, 38, 1991−2003.

[18] a) X. Li, Q. Song, L. Hao, L. Zhi, *Small* **2014**, 10, 2122−2135; b) S. N. Talapaneni, T. H. Hwang, S. H. Je, O. Buyukcakir, J. W. Choi, A. Coskun, *Angew. Chem. Int. Ed.* **2016**, 55, 3106−3111; *Angew. Chem.* **2016**, 128, 3158−3163.

[19] Y. H. Cho, C.−Y. Lee, D.−C. Ha, C.−H. Cheon, *Adv. Synth. Catal.* **2012**, 354, 2992−2996.

[20] a) D. A. Pyles, J. W. Crowe, L. A. Baldwin, P. L. McGrier, *ACS Macro Lett.* **2016**, 5, 1055−1058; b) P.-F. Wei, M.-Z. Qi, Z.-P. Wang, S.-Y. Ding, W. Yu, Q. Liu, L.-K. Wang, H.-Z. Wang, W.-K. An, W. Wang, *J. Am. Chem. Soc.* **2018**, 140, 4623−4631.

[21] H. Ataee-Esfahani, Y. Nemoto, L. Wang, Y. Yamauchi, *Chem. Commun.* **2011**,47, 3885−3887.

[22] S. Ghosh, M. Reches, E. Gazit, S. Verma, *Angew. Chem. Int. Ed.* **2007**, 46, 2002−2004.

[23] G. Kim, J. Yang, N. Nakashima, T. Shiraki, *Chem. Eur. J.* **2017**, 23, 17504−17510.

[24] a) F. Hu, J. Wang, S. Hu, L. Li, W. Shao, J. Qiu, Z. Lei, W. Deng, X. Jian, *ACS Appl. Mater. Interfaces* **2017**, 9, 31940−31949; b) Y. Jia, Y. Lin, Y. Ma, W. Shi, *Mater. Des.* **2018**, 160, 1071−1079.

[25] a) P. Bhanja, K. Bhunia, S.K. Das, D. Pradhan, R. Kimura, Y. Hijikata, S. Irle, A. Bhaumik, *ChemSusChem* **2017**, 10, 921−929; b) S.K. Das, K. Bhunia, A. Mallick, A. Pradhan, D. Pradhan, A. Bhaumik, *Microporous Mesoporous Mater.* **2018**, 266, 109−116.

[26] a) 9 X. Yu, J. Zhao, R. Lv, Q. Liang, C. Zhan, Y. Bai, Z.-H. Huang, W. Shen and F. Kang, *J. Mater. Chem. A,* **2015**, 3, 18400–18405; b) L.-P. Lv, Z.-S. Wu, L. Chen, H. Lu, Y.-R. Zheng, T. Weidner, X. Feng, K. Landfester and D. Crespy, *RSC Adv.,* **2015**, 5, 50063–50069; c) S. Zhang, A. Ikoma, K. Ueno, Z. Chen, K. Dokko and M. Watanabe, *ChemSusChem,* **2015**, 8, 1608–1617; d) M. Zhong, E. K. Kim, J. P. McGann, S.-E. Chun, J. F. Whitacre, M. Jaroniec, K. Matyjaszewski and T. Kowalewski, *J. Am. Chem. Soc.,* **2012**, 134, 14846–14857.

10.1002/asia.201900296

WILEY-VCH

Microtubular supercapacitor: planar tris(4-formylphenyl)triazine and 2,5-diaminohydroquinone have been integrated into a hollow microtubular triazine- and benzobisoxazole-based covalent organic framework with a sponge-like shell by means of a template-free [3+2] condensation. Upon application, the resultant COF exhibited a significant supercapacitor performance.

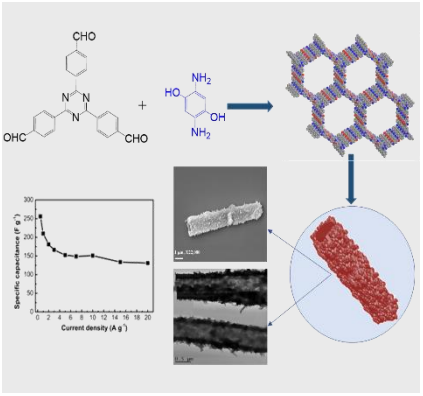

*Ahmed F. M. EL-Mahdy, Ying-Hui Hung, Tharwat Hassan Mansoure, Hsiao-Hua Yu, Tao Chen, Shiao-Wei Kuo**

Page No. – Page No.

A Hollow Microtubular Triazine- and Benzobisoxazole-Based Covalent Organic Framework Presenting Sponge-Like Shells That Functions as a High-Performance Supercapacitor